PAPER

Check for updates

The one/two atom size-reduction of [Au$_{23}$SCy$_{16}$]$^−$ induced by the [Au$_6$(dppp)$_4$]$^{2+}$ cluster†

Lichao Zhang, [ab] Daoqing Fan, [a] Yanan Shi, [a] Shuping He, [a] Mengting Cui, [a] Haizhu Yu [*ab] and Manzhou Zhu [a]

The recent progress in atomically precise metal (Au, Ag etc.) nanoclusters has greatly enriched the molecular-level mechanistic understanding of metal nanomaterials. Herein, using two meta-stable (easy formation, easy transformation) clusters, i.e. [Au$_{23}$SCy$_{16}$]$^−$ and [Au$_6$(dppp)$_4$]$^{2+}$ (HSCy and dppp denote cyclohexanethiol and 1,3-bis(diphenylphosphino)propane), as the reaction precursors, the etching of Au$_{23}$ occurs smoothly, giving the one/two-atom size-reduced [Au$_{21}$SCy$_{12}$(dppp)$_2$]$^+$ and [Au$_{22}$SCy$_{14}$(dppp)]$^{2+}$ as the major products. Structural analysis and DFT calculations indicate that the active reaction site of Au$_{23}$ lies in the core−shell interference of the bi-capped icosahedral Au$_{15}$ core and the AuS$_2$ motifs. The fluorescence, band gap, and thermostability of the Au$_{21}$ cluster products are improved compared to that of the Au$_{23}$ precursors.

Introduction

The atomic precision of noble metal nanoclusters (with single crystal X-ray diffraction, mass spectra etc.) makes it possible to elucidate the fantastic chemistry and the inherent structure–property correlations of nanomaterials at a molecular level.[1–3] The stimuli response (to pH changes, additives etc.[4]) represents one of the most appealing characteristics of metal nanoclusters, providing sound proof for the traditional theories (such as the Lamer/aggregative size growth),[5] and opening the door for the practical applications in catalysis,[6,7] sensing[8,9] and bioclinics.[10] In this scenario, the inter-cluster reactions have become a novel synthetic strategy to prepare atomically precise metal nanoclusters,[11] and to shed light on the dynamics of the cluster precursors.

So far, most of the reported inter-cluster reactions feature ligand exchange or/and metal exchange characteristics. Typically, the size-maintained ligand exchange occurs between two cluster analogs bearing different ligands, such as the reaction of [Au$_{25}$(PET)$_{18}$]$^−$ with [Au$_{25}$(SBut)$_{18}$]$^−$ (HPET and HSBut are short for 2-phenyl ethanethiol and 1-butanethiol),[12] and the reaction of [Au$_{25}$(SC$_{10}$H$_{21}$)$_{18}$]$^−$ with [Au$_{25}$(SC$_{12}$H$_{25}$)$_{18}$]$^−$ (linear alkyl thiolates

in both cases).[13] Meanwhile, the metal exchange has been widely reported in the interparticle reactions between two clusters of different metal components (or isotopic ones). For example, the size- and framework-maintained metal exchange occurs in the reaction of [Ag$_{25}$(DMBT)$_{18}$]$^−$ with [Au$_{25}$(PET)$_{18}$]$^−$,[14] [Ag$_7$(H){S$_2$P(O^{i}Pr)$_2$}$_6$] with [Cu$_7$(H){S$_2$P(O^{i}Pr)$_2$}$_6$],[15] and the isotopic exchange reactions of [$^{107/109}$Ag$_{25}$(DMBT)$_{18}$]$^−$ (ref. 16) and [$^{107/109}$Ag$_{29}$(BDT)$_{12}$(TPP)$_4$$^{3−}$].[17] Of note, the inter-cluster reactions between two structurally distinct clusters have also been reported. In the pioneering studies, the reaction of [Au$_{25}$(FTP)$_{18}$]$^−$ with [Ag$_{44}$(FTP)$_{30}$]$^{3−}$,[18] [Au$_{25}$(PET)$_{18}$]$^−$ with [Ir$_9$(PET)$_6$]$^+$ (ref. 19) and [Au$_{25}$(SBut)$_{18}$]$^−$ with [Ag$_{51}$(BDT)$_{19}$(TPP)$_3$]$^{3−}$ (ref. 20) each generates an alloy cluster product with the same framework as one of the precursors. The distinct metal components and the predominant doping processes in these reactions arise an interesting question as to the reaction mode between two same-metal clusters. To our knowledge, only one such reaction has been reported, i.e. the formation of [Ag$_{16}$(TBT)$_8$(TFA)$_7$(CH$_3$CN)$_3$Cl]$^+$ and [Ag$_{17}$(TBT)$_8$(TFA)$_7$(CH$_3$CN)$_3$Cl]$^+$ cocrystals via the reaction of [Ag$_{12}$(TBT)$_8$(TFA)$_5$(CH$_3$CN)]$^+$ and [Ag$_{18}$(TPP)$_{10}$H$_{16}$]$^{2+}$ (TBT = tert-butylthiolate, TFA = trifluoroacetate, CH$_3$CN = acetonitrile, TPP = triphenylphosphine).[21] The structure of the co-crystalized Ag$_{16}$ and Ag$_{17}$ products are distinct from the precursors.

Inspired by the inter-particle reaction of the two Ag clusters bearing totally different ligands, herein we chose [Au$_{23}$SCy$_{16}$]$^−$ and [Au$_6$(dppp)$_4$]$^{2+}$ (abbreviated as Au$_{23}$ and Au$_6$) as the reactants. Both of them are meta-stable (easy formation, easy transformation). The single crystal structure of Au$_6$ [22] and Au$_{23}$ [23] has been reported, demonstrating their stability during synthesis and under crystallization conditions. But on the other hand, Au$_6$ easily react with the Au(ɪ) complex or Ag$^+$ salt to generate [Au$_8$(dppp)$_4$Cl$_2$]$^{2+}$,[24] or [Au$_7$(dppp)$_4$]$^{3+}$.[25] While upon heating or oxidation with H$_2$O$_2$, Au$_6$

^{a}Department of Chemistry and Centre for Atomic Engineering of Advanced Materials, Key Laboratory of Structure and Functional Regulation of Hybrid Materials of Physical Science and Information Technology and Anhui Province Key Laboratory of Chemistry for Inorganic/Organic Hybrid Functionalized Materials, Anhui University, Hefei 230601, China. E-mail: yuhaizhu@ahu.edu.cn

^{b}Institute of Energy, Hefei Comprehensive National Science Center, Hefei 230601, China

easily converts to $[Au_{11}(dppp)_5]^{3+}$ or $[Au_8(dppp)_4Cl_2]^{2+}$.[26] Similarly, rich chemistry has been reported for the Au_{23} clusters. The addition of different thiolate ligands (TBBzT/TBBT/2-NPT) results in the size-growth of Au_{23} to $Au_{24}/Au_{25}/Au_{28}$,[27,28] while the addition of phosphine ligand results in a distinct size-reduction of $Au_{23} \rightarrow Au_{22}$ (ref. 29 and 30)/Au_{21}.[30] Meanwhile, the addition of MSCy (M = Ag/Au) complexes results in the formation of heavily Ag-doped alloy $(AuAg)_{25}$[31] and Au_{28},[32] respectively. Of note, the $Au_{23} \rightarrow Au_{28}$ conversion has also been regulated by oxidation[33] and photooxidation[34] conditions. In this context, the reaction of Au_6 with Au_{23} clusters will aid the elucidation on the relative stability of the two cluster precursors, and shed light on the inherent structure–activity relationships therein.

In this study, the inter-cluster reaction of $[Au_{23}SCy_{16}]^-$ with $[Au_6(dppp)_4]^{2+}$ were conducted. In an equimolar reaction of Au_{23} and Au_6, two main products, *i.e.* $[Au_{21}SCy_{12}(dppp)_2]^+$ (Au_{21}), and $[Au_{22}SCy_{14}(dppp)]^{2+}$ (Au_{22} for short) were identified and characterized by ESI-MS and UV-vis *etc.* The framework of Au_{23} is largely maintained in Au_{22} and Au_{21}, while the one or two groups of $Au(SCy)_2$ motifs were each replaced by a dppp ligand. With the combination of DFT and structural analysis, the active etching site on the Au_{23} precursor was found to be the $Au(core)$-$S(on AuS_2$ motif) bonds. Meanwhile, replacing the AuS_2 motifs with the dppp ligands results in significantly higher luminescence, a relatively larger O1–R1 gap, and higher thermal stability.

Experimental

Materials

All reagents were commercially available and used without further purification: dichloromethane (CH_2Cl_2, HPLC grade, ≥99.9%), methanol (MeOH, HPLC grade, ≥99.9%), *n*-hexane (*n*-Hex, HPLC grade, ≥98.0%) $HAuCl_4 \cdot 4H_2O$ (≥99.99%, metal basis), and cyclohexane-thiol (HSCy, ≥98%), sodium borohydride ($NaBH_4$, ≥98%), tetrabutylammonium bromide (TOABr, ≥99%), 1,3-bis(diphenylphosphine)propane (≥98%) were purchased from Shanghai Macklin Biochemical Co., Ltd. All glassware was thoroughly cleaned with aqua regia (HCl/HNO_3 3/ 1 v/v), rinsed with copious amounts of pure water, and then dried in an oven before use.

Synthesis of $[Au_{23}SCy_{16}]^-$ and $[Au_6(dppp)_4]^{2+}$

$[Au_{23}SCy_{16}]^-$ and $[Au_6(dppp)_4]^{2+}$ were prepared *via* the previously reported methods,[35,36] and verified by UV-vis, and ESI-MS analysis (please see supporting information Fig. S1 and S2†). Briefly, Au_{23} was synthesized by adding HSCy, TOAB, and $NaBH_4$ into the aqueous solution of $HAuCl_4$ in methanol, and $[Au_6(dppp)_4]^{2+}$ was formed *via* the reaction of $HAuCl_4$, dppp and $NaBH_4$ under room temperature in ethanol.

Characterization

UV-vis absorption spectra were recorded on a UV-6000PC instrument. All fluorescence spectra were obtained using a HORIBA FluoroMax-4P fluorescence spectrophotometer.

Electrospray ionization mass spectrometry measurement was recorded using a Waters Xevo G2-XS QT mass spectrometer.

Results and discussion

The reaction of $[Au_{23}SCy_{16}]^-$ and $[Au_6(dppp)_4]^{2+}$

The reaction of $[Au_{23}SCy_{16}]^-$ and $[Au_6(dppp)_4]^{2+}$ was conducted in a 1 : 1 molar ratio. In detail, 20 mg $[Au_{23}SCy_{16}]^-$ was dissolved in 15 mL of DCM, and then 8.3 mg of $[Au_6(dppp)_4]^{2+}$ was added. Stirring for about 3 hours, the solution colour changed from brownish black to crimson black (Fig. 1a). The crude product was then concentrated and purified by preparative thin-layer chromatography (abbreviated as PTLC) with DCM/Hex (1 : 2) for the first time, and by PTLC with DCM/MeOH (10 : 1) for the second time (Fig. 1b inset).

According to Fig. 1b, the UV-vis spectra of the DCM solution of the two bands are very similar, each of which shows a prominent peak at ~570 nm, and a shoulder peak at ~460 nm. Meanwhile, ESI-MS characterization of the band I component shows a prominent cluster peak at $m/z = 3179.37$, corresponding to $[Au_{22}SCy_{14}(dppp)]^{2+}$ (Fig. 2a). The ESI-MS of the band II component shows a cluster peak at $m/z = 6343.40$ (Fig. 2b), corresponding to a cluster formula of $[Au_{21}SCy_{12}(dppp)_2]^+$ (Au_{21} for short). For both Au_{22} and Au_{21}, the isotopic pattern is in excellent agreement with the theoretical one (Fig. 2a and b inset).

Of note, the UV-vis spectra of the formed Au_{21} and Au_{22} clusters are very similar to the reported spectra of $[Au_{22}SCy_{14}(dppp)]$, and $[Au_{21}SCy_{12}L_2]^+$ (L = dppm/dppe/CDPE).[30] But the conversion details and the components of the Au_{21} and Au_{22} clusters are distinct from the reported ones. First, the reported Au_{21} and Au_{22} clusters were formed *via* the Au^IL (L = diphosphate) etching of Au_{23} precursor, while the inter-cluster reaction of Au_{23} and Au_6 was used in this study. Second, the charge state of the Au_{22}
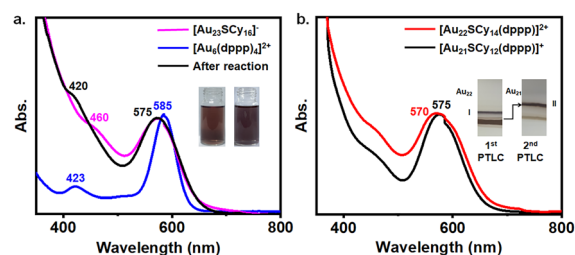

Fig. 1 The UV-vis spectra of the Au_{23}, Au_6 precursors and the solution after reacting for 3 hours (a), inset: digital photo of the reaction solution before (left) and after reaction (right); and the UV-vis of the different band components after PTLC separation (b) insets: digital photo of the band distribution.
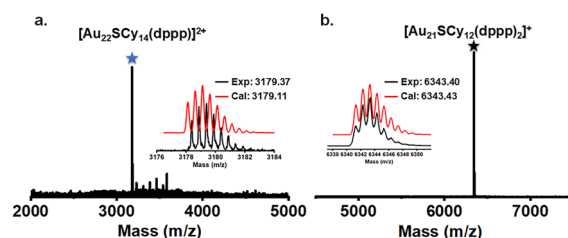

Fig. 2 The ESI-MS and the correlation of the experimental isotopic pattern with the theoretical one (inset) of Au_{22} (a) and Au_{21} clusters (b).
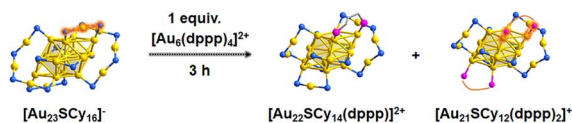
Fig. 3 The size-conversion of the $[Au_{23}SCy_{16}]^-$ and $[Au_6(dppp)_4]^{2+}$ clusters with the related structures.

Fig. 4 Emission spectra of Au_{23}, Au_{22} and Au_{21} under excitation upon 365 nm light irradiation.

clusters in this study is distinct from the reported one (+2 *vs.* 0). Besides, the Au_{21} cluster co-protected by SCy and dppp ligands was not reported,[30] and the etching of Au_{23} with Au^Idppp generates Au_{22} cluster exclusively in the early study. Herein, using Au_6 as a dppp-donating reagent, the Au_{21} cluster co-protected by SCy and dppp ligand was gained as a main product. Nevertheless, given the similarity in the UV-vis of the formed Au_{22}/Au_{21} cluster with the reported ones, and the plausibility of using UV-vis absorption curve to determine the cluster frameworks,[35,36] we anticipated that the framework of the formed Au_{21} and Au_{22} clusters is similar to the reported ones. Accordingly, the structure of the $[Au_{23}SCy_{16}]^-$ has been largely maintained after the reaction.

As shown in Fig. 3, the structure of Au_{23} could be viewed as protecting the bicapped icosahedral Au_{15} core with two Au_3S_4, two AuS_2 staple motifs, and four bridging thiolate ligands. Replacing one or two AuS_2 motifs with one/two dppp ligands generates the structure of Au_{22}/Au_{21}. On the basis of the structural analysis, we performed density functional theory (DFT) calculations on the bond dissociation energy (BDE) of the Au–S bonds (see ESI† for the details of the computational method). The detailed results are given in Fig. S3,† and the BDE of the Au–S bonds between Au_{15} core and S on AuS_2 is remarkably lower than all other ones, while the Au^{cap}–S bond (Fig. 3) is slightly lower than that of the Au^{core}–S (8.1 *vs.* 10.8 kcal mol^{-1}). According to the calculation results, both bonds could be easily broken under experimental conditions due to the low energy demands.

Given the reaction mechanism, PTLC monitoring on the target reaction system (Fig. S4†) indicates the rapid formation of Au_{22} and Au_{21} within the first 10 minutes. After that, the amount of the Au_{22} slightly diminished in the following reaction time. By contrast, the amount of Au_{21} gradually increased, associated with the continuous reduction of both Au_{22} and the Au_6 components. The results imply the easy replacement of the first AuS_2 motif, but the relatively difficult replacement of the second AuS_2 motif on the Au_{23} precursor. In other words, the reactivity for the ligand exchange of AuS_2 to dppp has been greatly reduced after the first time exchange.

Fluorescence

Albeit the similar framework, $[Au_{23}(SCy)_{16}]^-$ showed a weak emission peak at 703 nm, while $[Au_{22}SCy_{14}(dppp)]^{2+}$ and $[Au_{21}SCy_{12}(dppp)_2]^+$ showed approximately 2-fold emission enhancement, with a tiny redshift of the emission maximum wavelength (708 nm for Au_{22} and 707 nm for Au_{21}, Fig. 4).

Differential pulse voltammetry (DPV)

The differential pulse voltammetry (DPV) curves of both Au_{23} precursor and the Au_{22}/Au_{21} product clusters (Fig. 5) feature
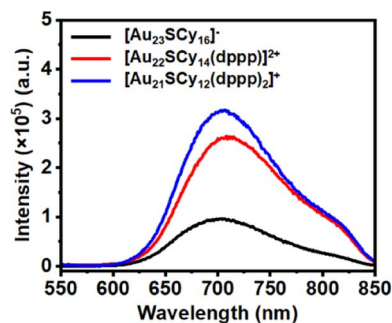
molecular-like electrochemical characteristics, with distinctive oxidation and reduction potentials. In detail, the first oxidation peaks (O1) of the Au_{23}, Au_{22} and Au_{21} clusters are at 0.13, 0.23 and 0.66 V, respectively. The first reduction peaks (R1) are observed at -0.78, -1.00 and -0.80 V, respectively. Accordingly, the R1–O1 gap of the Au_{23}, Au_{22} and Au_{21} clusters are 0.91, 1.23 and 1.46 V, respectively. The enlarged gap of Au_{22} and Au_{21} than that of Au_{23} demonstrates the enhanced electrochemical stability induced by the $AuS_2 \rightarrow$ dppp exchange.

Thermal stability

Associating with the size-reduction, the thermal stability of the clusters has been significantly improved. Following the recent studies,[37,38] the stability of the Au_{21}, Au_{22} and Au_{23} clusters under heating conditions were tracked with the UV-vis spectrum. As shown in Fig. 6, upon heating at 60 °C, the characteristic peak on UV-vis spectra of Au_{22} and Au_{21} maintains after even 18 hours, and the Au_{21} cluster is even stable after 60 hours. By contrast, the characteristic peak of Au_{23} attenuated within 1 hour, and becomes very weak after 18 hours. Herein, both the
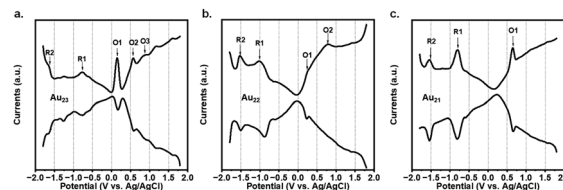

Fig. 5 DPV spectra of Au_{23} (a), Au_{22} (b) and Au_{21} (c) in 0.1 M Bu_4NPF_6–CH_2Cl_2 solutions that are degassed for 15 min and blanketed with N_2 at room temperature. Open-circuit voltage is 0.204 V.
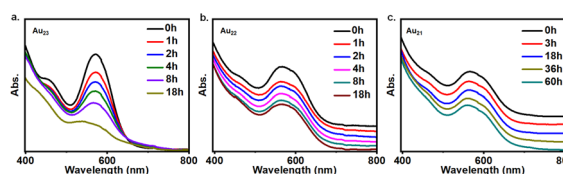

Fig. 6 Thermal stability test of Au_{23} (a), Au_{22} (b) and Au_{21} (c) clusters at 60 °C in toluene.

higher thermal stability and the co-presence of thiolate and diphosphine ligands will be helpful for the future application of the Au_{22}/Au_{21} clusters.

Conclusions

Herein, the inter-cluster reaction of $[Au_{23}SCy_{16}]^-$ and $[Au_6(dppp)_4]^{2+}$ clusters were conducted. $[Au_{21}SCy_{12}(dppp)_2]^+$, and $[Au_{22}SCy_{14}(dppp)]^{2+}$ were identified as the main products. The preliminary mechanistic insights with the combination of experimental and DFT calculations indicates the Au–S bond in the core–shell interference, and especially the Au–S bond of AuS_2 motif and the core structure, is the active reaction site. After incorporating the diphosphine ligands, the Au_{22}/Au_{21} clusters show stronger luminescence than the Au_{23} precursor. Meanwhile, both the electrochemical and thermo-stability tests indicate the higher stability of the Au_{21} than that of the Au_{23} precursors. The enhanced stability of the produced clusters might show high potential in future applications.

Author contributions

All authors have given approval to the final version of the manuscript. L. Z.: experiments, data analysis, manuscript draft; D. F.: investigation, formal analysis; M.C.: initial experiments; S. H. and Y. S.: theoretical calculation; H. Y.: conceptualization, supervision, review & editing, funding acquisition; M. Z.: conceptualization, supervision.

Conflicts of interest

There are no conflicts to declare.

Acknowledgements

References

1 J. Yang, Y. Peng, S. Li, J. Mu, Z. Huang, J. Ma, Z. Shi and Q. Jia, *Coord. Chem. Rev.*, 2022, **456**, 214391.

2 X. Kang, H. Chong and M. Zhu, *Nanoscale*, 2018, **10**, 10758–10834.

3 K. A. Benavides, I. W. H. Oswald and J. Y. Chan, *Acc. Chem. Res.*, 2018, **51**, 12–20.

4 M. Waszkielewicz, J. Olesiak-Banska, C. Comby-Zerbino, F. Bertorelle, X. Dagany, A. K. Bansal, M. T. Sajjad, I. D. W. Samuel, Z. Sanader, M. Rozycka, M. Wojtas, K. Matczyszyn, V. Bonacic-Koutecky, R. Antoine, A. Ozyhar and M. Samoc, *Nanoscale*, 2018, **10**, 11335–11341.

5 Q. Yao, X. Yuan, V. Fung, Y. Yu, D. T. Leong, D. Jiang and J. Xie, *Nat. Commun.*, 2017, **8**, 927.

6 Y. Li, S. Li, A. V. Nagarajan, Z. Liu, S. Nevins, Y. Song, G. Mpourmpakis and R. Jin, *J. Am. Chem. Soc.*, 2021, **143**, 11102–11108.

7 B. Kim, H. Seong, J. T. Song, K. Kwak, H. Song, Y. C. Tan, G. Park, D. Lee and J. Oh, *ACS Energy Lett.*, 2020, **5**, 749–757.

8 L. Shang, J. Xu and G. U. Nienhaus, *Nano Today*, 2019, **28**, 100767.

9 X. Song, N. Goswami, H. Yang and J. Xie, *Analyst*, 2016, **141**, 3126–3140.

10 Z. Qiao, J. Zhang, X. Hai, Y. Yan, W. Song and S. Bi, *Biosens. Bioelectron.*, 2021, **176**, 112898.

11 E. Khatun, P. Chakraborty, B. R. Jacob, G. Paramasivam, M. Bodiuzzaman, W. A. Dar and T. Pradeep, *Chem. Mater.*, 2019, **32**, 611–619.

12 G. Salassa, A. Sels, F. Mancin and T. Burgi, *ACS Nano*, 2017, **11**, 12609–12614.

13 Y. Niihori, W. Kurashige, M. Matsuzaki and Y. Negishi, *Nanoscale*, 2013, **5**, 508–512.

14 M. Neumaier, A. Baksi, P. Weis, E. K. Schneider, P. Chakraborty, H. Hahn, T. Pradeep and M. M. Kappes, *J. Am. Chem. Soc.*, 2021, **143**, 6969–6980.

15 Y.-J. Zhong, J.-H. Liao, T.-H. Chiu, Y.-Y. Wu, S. Kahlal, M. J. McGlinchey, J.-Y. Saillard and C. W. Liu, *Dalton Trans.*, 2021, **50**, 4727–4734.

16 P. Chakraborty, P. Bose, J. Roy, A. Nag, B. Mondal, A. Chakraborty and T. Pradeep, *J. Phys. Chem. C*, 2021, **125**, 16110–16117.

17 P. Chakraborty, A. Nag, G. Natarajan, N. Bandyopadhyay, G. Paramasivam, M. K. Panwar, J. Chakrabarti and T. Pradeep, *Sci. Adv.*, 2019, **5**, eaau7555.

18 K. R. Krishnadas, A. Baksi, A. Ghosh, G. Natarajan and T. Pradeep, *ACS Nano*, 2017, **11**, 6015–6023.

19 G. Hou, C. Liu, R.-Z. Li, H. Xu, Y. Q. Gao and W. Zheng, *J. Phys. Chem. Lett.*, 2017, **8**, 13–20.

20 A. Ghosh, D. Ghosh, E. Khatun, P. Chakraborty and T. Pradeep, *Nanoscale*, 2017, **9**, 1068–1077.

21 W. A. Dar, M. Bodiuzzaman, D. Ghosh, G. Paramasivam, E. Khatun, K. S. Sugi and T. Pradeep, *ACS Nano*, 2019, **13**, 13365–13373.

22 J. W. A. Van der Velden, J. J. Bour, J. J. Steggerda, P. T. Beurskens, M. Roseboom and J. H. Noordik, *Inorg. Chem.*, 1982, **21**, 4321–4324.

23 A. Das, T. Li, K. Nobusada, C. Zeng, N. L. Rosi and R. Jin, *J. Am. Chem. Soc.*, 2013, **135**, 18264–18267.

24 Y. Kamei, Y. Shichibu and K. Konishi, *Angew. Chem., Int. Ed.*, 2011, **50**, 7442–7445.

25 Y. Shichibu, M. Zhang, Y. Kamei and K. Konishi, *J. Am. Chem. Soc.*, 2014, **136**, 12892–12895.

26 X. Ren, J. Fu, X. Lin, X. Fu, J. Yan, R. Wu, C. Liu and J. Huang, *Dalton Trans.*, 2018, **47**, 7487–7491.

27 M. P. Maman, A. S. Nair, A. M. A. H. Nazeeja, B. Pathak and S. Mandal, *J. Phys. Chem. Lett.*, 2020, **11**, 10052–10059.

28 M. P. Maman, A. S. Nair, H. Cheraparambil, B. Pathak and S. Mandal, *J. Phys. Chem. Lett.*, 2020, **11**, 1781–1788.

29 Z. He, Y. Yang, J. Zou, Q. You, L. Feng, M.-B. Li and Z. Wu, *Chem. - Eur. J.*, 2022, **28**, e202200212.

30 Q. Li, S. Yang, J. Chai, H. Zhang and M. Zhu, *Nanoscale*, 2022, **14**, 15804–15811.

31 Q. Li, S. Wang, K. Kirschbaum, K. J. Lambright, A. Das and R. Jin, *Chem. Commun.*, 2016, **52**, 5194–5197.

32 N. Xia, J. Yuan, L. Liao, W. Zhang, J. Li, H. Deng, J. Yang and Z. Wu, *J. Am. Chem. Soc.*, 2020, **142**, 12140–12145.

33 T. Higaki, C. Liu, Y. Chen, S. Zhao, C. Zeng, R. Jin, S. Wang, N. L. Rosi and R. Jin, *J. Phys. Chem. Lett.*, 2017, **8**, 866–870.

34 L. Tang, X. Kang, S. Wang and M. Zhu, *Langmuir*, 2019, **35**, 12350–12355.

35 X. Lin, C. Liu, K. Sun, R. Wu, X. Fu and J. Huang, *Nano Res.*, 2019, **12**, 309–314.

36 X. Liu, W. Xu, X. Huang, E. Wang, X. Cai, Y. Zhao, J. Li, M. Xiao, C. Zhang, Y. Gao, W. Ding and Y. Zhu, *Nat. Commun.*, 2020, **11**, 3349.

37 Z.-J. Guan, J.-L. Zeng, S.-F. Yuan, F. Hu, Y.-M. Lin and Q.-M. Wang, *Angew. Chem., Int. Ed.*, 2018, **57**, 5703–5707.

38 X. Fu, X. Lin, X. Ren, H. Cong, C. Liu and J. Huang, *Chin. Chem. Lett.*, 2021, **32**, 565–568.